Article

A Cippus from Turris Libisonis: Evidence for the Use of Local Materials in Roman Painting on Stone in Northern Sardinia

Roberta Iannaccone [1,2,*], Stefano Giuliani [3], Sara Lenzi [4], Matteo M. N. Franceschini [1,5], Silvia Vettori [1] and Barbara Salvadori [1]

1 Institute of Heritage Science, National Research Council of Italy (ISPC-CNR), Via Madonna del Piano 10, 50019 Florence, Italy; matteomaria.franceschini@uniroma1.it (M.M.N.F.); silvia.vettori@cnr.it (S.V.); barbara.salvadori@cnr.it (B.S.)
2 Department of Chemical, Physical, Mathematical and Natural Sciences, University of Sassari, Via Vienna 2, 07100 Sassari, Italy
3 Direzione Regionale Musei Sardegna, Complesso Monumentale ex SS. Annunziata, Corso Francesco Cossiga, 07100 Sassari, Italy; stefano.giuliani@cultura.gov.it
4 Department of History, Archaeology and Art History, Università Cattolica del Sacro Cuore, Largo Gemelli 1, 20123 Milan, Italy; sara.lenzi1@unicatt.it
5 Department of Science of Antiquities, Sapienza University of Rome, Piazzale Aldo Moro 5, 00185 Rome, Italy
* Correspondence: robertaiannaccone@cnr.it

Abstract: The ancient Roman town of Turris Libisonis was located on the northern coast of Sardinia and was known in the past as an important naval port. Located in the Gulf of Asinara, it was a Roman colony from the 1st century BCE and became one of the richest towns on the island. Among the archaeological finds in the area, the cippus exhibited in the Antiquarium Turritano is of great interest for its well-preserved traces of polychromy. The artefact dates back to the early Imperial Age and could have had a funerary or votive function. The artefact was first examined using a portable and non-invasive protocol involving multi-band imaging (MBI), portable X-ray fluorescence (p-XRF), portable FT-IR in external reflectance mode (ER FT-IR) and Raman spectroscopy. After this initial examination, a few microfragments were collected and investigated by optical microscopy (OM), X-ray powder diffraction (XRPD), Fourier-transform infrared spectroscopy in ATR mode (ATR FT-IR) and micro-ATR mode (μATR FT-IR) and Scanning Electron Microscopy/Energy Dispersive Spectroscopy (SEM-EDS) to improve our knowledge and characterize the materials and to determine their provenience. The results contribute to a better understanding of the provenance of materials and shed light on pigments on stone and their use outside the Italian peninsula and, in particular, Roman Sardinia.

Keywords: Roman Sardinia; Turris Libisonis; Porto Torres; Roman painting; cippus; multimethodological approach; pigment characterization; stone provenance

1. Introduction

The ancient Roman town of Turris Libisonis [1] was located on the northern coast of Sardinia, not far from the modern city of Sassari. Turris Libisonis (nowadays known as Porto Torres) was a fundamental seaport in ancient times, and was located in the Asinara Gulf.

According to Plinius the Elder, it was the sole colony in Roman Sardinia [2]. Its foundation is attributed to Julius Caesar or Octavian before 27 BCE (as evidenced by the cognomen "Iulia"—Colonia Iulia Turris Libisonis) [3].

The city reached its peak from the 2nd century CE onwards, and had a period of prosperity particularly during the mid-3rd century CE, when some important buildings were constructed including baths, a basilica, temples, etc.

The main feature of the city was its port, which attests to the significance of the maritime trade with Ostia. This is evidenced by the stylistic influence on the sculptural

production and mosaics and the presence of the *statio* of the *navicularii turritani* in the *Foro delle Corporazioni* in Ostia at the end of the 2nd century CE [4].

The materials from the port, particularly the *anforae*, demonstrate a comprehensive involvement of the city and the Sardinian territory in the Mediterranean Sea trade. This was evidenced by the city's role as a collector of Sardinian cereals and minerals for Rome, as well as its status as an important transit point on routes from Rome to Africa, Spain and Gaul. However, there is limited evidence to suggest that Oriental imports were a significant aspect of this trade [5].

The seaport was the starting point (*caput viae*) of the entire road network in Roman Sardinia, and the road axes which were used for the transportation of cereals towards the port were reconstructed until the end of the 4th century CE.

The topography of the ancient city is still not well known, since the remains of the Roman Turris Libisonis lie under the modern town of Porto Torres and the forum has never been identified with certainty.

Three important baths have been found: the Pallottino Baths, the Central Baths (also known as the "Palazzo di Re Barbaro") and the Maetzke Baths. Other buildings that have survived to the present day include two domus (the "Domus di Orfeo" and the "Domus dei Mosaici Marini"), a section of the city walls from the Imperial Age and the bridge with seven arches over the river Riu Mannu. Some buildings are known from epigraphic documentation, including the Basilica, the Tribunal and the Temple of Fortuna, but the city probably also had an *Iseum*, an *Augusteum*, the *Capitolium* and a *Mitraeum*. Few remains of the aqueduct that collected water from the hills around the nearby modern city of Sassari are known [6].

Nowadays, only a part of ancient Turris Libisonis has been unearthed and is visible in the archaeological site located near the modern Antiquarium Turritano, which was opened to the public in 1984 [7].

Between 2006 and 2007, an enlargement of the modern port of Porto Torres was undertaken in order to facilitate the docking of ferries arriving from the Italian Peninsula. The old pier of the lighthouse was destroyed and thousands of archaeological materials of ancient Turris Libisonis came to light [8].

The archaeological research showed that a considerable number of the ancient objects were not in their original context, and they probably came from the destruction of Roman buildings that took place in modern times, between the 19th and the beginning of the 20th century when the city of Porto Torres was improved with new infrastructure [8,9]. Then, the ruins of the Roman buildings and thousands of ancient objects were re-used to fill the foundations of the pier of the lighthouse.

Among the artefacts rediscovered in the area, a small group of Roman cippi with extensive traces of ancient painting was of particular interest. One of them was restored, exhibited at the Antiquarium Turritano and published by Gabriella Gasperetti [8].

This study, one of the first to examine polychromy in Roman Sardinia, aims to shed light on an unusual object: a Roman stone cippus covered with painted plaster that lacks well-known comparisons and exhibits good preservation despite prolonged immersion in seawater.

The archaeological study prompted questions regarding the provenance of the stone and pigments (local or imported), and the possibility of an inscription on the surface of the *tabella ansata* or a drawing on the white background on the other surviving side.

In order to answer these questions and to obtain a comprehensive characterization of the materials in question, a serie of analyses was carried out. Given its burial location, the cippus exhibits considerable damage, with an ongoing degradation process still evident. Accordingly, the analytical protocol employed portable and non-invasive techniques. The decision was made, in accordance with the museum, to proceed with further analysis involving the sampling of three selected areas. This was deemed necessary to increase the knowledge base regarding the understanding of the conservation status of the artefact and to provide useful information for a possible restoration campaign.

2. Materials and Methods

The cippus, measuring approximately 80 × 50 cm, was carved from a single block of stone, yellowish in color. The stone was completely covered with a preparatory layer and then painted with bright colors, especially yellow, green and black. Traces of color are still visible on three sides of the stone, and the fourth side was probably painted as well. Two sides of the cippus still preserve the painting over almost the entire surface, while the third side shows only a small fragment in the lower part.

To facilitate the discussion, the two painted sides of the cippus are referred to as side A and side B (Figure 1).
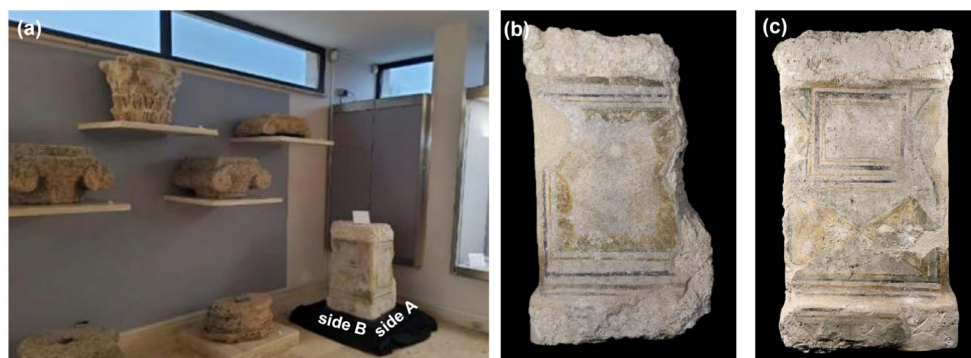
Figure 1. (**a**) The position of the cippus in the Antiquarium of Porto Torres (SS) and the two sides analyzed: (**b**) side A; (**c**) side B (courtesy of Ministero della Cultura–Direzione Regionale Musei Sardegna).

Side A is the side of the cippus that is directly visible to visitors to the exhibition and displays evidence of decoration with yellow, brown, red and white colors. The decoration is characterized by a lack of detail and accuracy; however, the white area is likely to represent a "tappeto teso" on a brownish yellow background. A possible comparison (but with different colors) is a painting from the Praedia of Iulia Felix in Pompeii (Museo Archeologico Nazionale di Napoli, inv. no. 8598) [10].

Side B shows geometric patterns, including a rectangle made up of four yellow and green triangles, as well as a *tabella ansata* with no visible inscription.

The decorations are framed by a series of green, yellow, black and greyish brown lines. The black and brown lines at the top and the bottom of the stone appear to imitate the moldings of similar marble and stone objects [11] using only color. The use of a chalk-line is visible, especially on side A.

According to previous studies, the chronology was set in the Early Imperial Age and its function could be either funerary or votive [8]. Its use as a base for sculptures was considered, like other examples with the same shape from Miseno [12]; however, the upper part of the object was too ruined to recognize any traces of a base for a sculpture. The purpose of the object, therefore, remains undetermined.

Both non-invasive and micro-invasive techniques were used to better understand the materials and degradation phenomena.

2.1. Non-Invasive Techniques

The non-invasive techniques used to investigate the cippus include the well-established in situ protocol of multiband imaging (MBI) and portable X-ray fluorescence (p-XRF) [13–15], together with the application of external reflection FT-IR (ER FT-IR) and Raman spectroscopy.

For the multiband imaging, a modified Nikon D850 (full frame sensor, 36 × 24 mm and 45.7 Mpixel) equipped with an AF-S Nikkor 24–120 VR f/4G ED VR lens (Nikon, Tokyo, Japan) was used for all wavelength ranges.

The correct combination between the radiation sources and the resulting wavelengths captured by the camera was obtained through the use of different filters. The combination of filters and sources employed for each technique is shown in Table 1.

Table 1. Combination of source and filters to achieve the image for every MBI technique.

Technique	Radiation Source	Filter on Camera Lens
Ultraviolet reflected photography—UVR	4 TL-D Blacklight Blue, 36 W BLB 1SL/25, Philips	X-Nite 330C + X-Nite PB1
Ultraviolet induced luminescence photography—UVL	4 TL-D Blacklight Blue, 36 W BLB 1SL/25	X-Nite CCI + Zeiss T* UV filter
Visible photography—VIS	2 Beghelli 16 W cold light 0120-Z	X-Nite CCI + Zeiss T* UV filter
Visible induced luminescence—VIL	2 Beghelli 16 W cold light 0120-Z	X-Nite 715
Near-infrared photography—NIR	2 Incandescent BR125, Philips	X-Nite 715
Near-infrared photography—NIR 1000	2 Incandescent BR125, Philips	X-Nite 1000
Raking light	2 Beghelli 16 W cold light 0120-Z	X-Nite CCI + Zeiss T* UV filter

The two techniques, called ultraviolet-reflected false color (UVFC) and infrared-reflected false color (IRFC), have been used as post-processing techniques since the introduction of digital photography [15,16]. The images were calibrated using an X-Rite Color Checker Passport Photo 2 (X-Rite, Grand Rapids, MI, USA).

The ER FT-IR measurements were acquired using an ALPHA FT-IR instrument (Bruker Optics, Ettingen, Germany) in the range from of 7500 to 375 cm^{-1}, with a resolution of 4 cm^{-1}, using a SiC Globar source and a DTGS detector equipped with an External Reflection module and a mask with a circular spot with a diameter of 5 mm. Spectra were acquired directly on the surface without sampling, with 128 scans collected for each measurement. The spectra were processed using OPUS 7.2 software [17].

Raman spectra were acquired using a Bravo spectrometer (Bruker Optics, Ettingen, Germany) equipped with two excitation lasers (DuoLaser™) with wavelengths ranging from 700 to 1100 nm and SSE™ technology to reduce fluorescence. The spectra were collected in two successive steps, from 300 cm^{-1} to 2000 cm^{-1} and from 2000 cm^{-1} to 3200 cm^{-1}, with each laser dedicated to one range only. The specified average spectral resolution was approximately 11 cm^{-1}, and the applied laser power was always less than 100 mW for both lasers [18]. The spectra were acquired with an integration time ranging from 500 ms to 1 s and accumulations from 4 to 32, and subsequently processed using OPUS 7.2 software.

Portable X-ray fluorescence (p-XRF) spectra were acquired using a portable Tracer IV SD (Bruker Optics, Germany) with a micro-X-ray tube, equipped with a rhodium anode and an SDD detector (FWHM < 145 eV at 100,000 cps). The spectra were acquired with the following parameters: 40 kV, 12 μA, no filter and an acquisition time of 60 s [19].

A portable USB microscope (OM) (Dino-Light, Torrance, CA, USA) with a magnification range from 20× to 200× was used to document both the surface of the cippus and the sampling areas. The images were acquired at high magnification, specifically 60× and 225×.

2.2. Micro-Invasive Techniques

Micro-invasive techniques were carried out in order to determine the petrographic and mineralogical composition of the stone and the preparation layer, and to better characterize the possible origin of the materials and the degradation phenomena that have occurred since its rediscovery.

SEM-EDS was performed using a Zeiss EVO LS10 Environmental Scanning Electron Microscope in low vacuum (LV) mode, without coating the sample that was mounted as is on a carbon stub. The analysis was performed under variable pressure (range 10–100 Pa) and the images were acquired using two detectors: a variable pressure secondary electron detector (VPSE) for secondary electrons (SE) and a backscattered electron detector

(BSD) for backscattered electrons (BSE). Elemental microanalysis was performed with an Inca X-Act Energy Dispersive Spectrometer (Oxford Instruments, Abingdon-on-Thamens, United Kingdom). The analysis was performed at 20 kV and 7.5 mm (working distance).

The stone and the mortar samples were analyzed by X-ray powder diffraction (XRPD) to characterize their mineralogical composition and by polarized transmitted light optical microscopy (OM) to obtain the petrographic characterization.

A PANalytical X'PertPRO X-ray diffractometer equipped with X'Celerator multi-revelatory and High Score 3.0d software for data acquisition and interpretation was used. The following operating conditions were used: $CuK\alpha1 = 1.54$ Å, current = 30 mA, voltage = 40 kV, 2θ range between $3°$ and $70°$, step size = $0.02°$ and time to step = 50 s (Malvern Panalytical Ltd., Malvern, United Kingdom).

The petrographic investigation was carried out using observations of thin sections (30 μm thickness) in transmitted light using an optical microscope (ZEISS Axioscope A1 microscope) equipped with a camera (resolution: 5 megapixels) and image analysis software (AxioVision 4.8.2) was used to evaluate the compositional and microstructural parameters (Carl Zeiss Microscopy, Jena, Germany).

FT-IR micro-ATR measurements on the green fragment were carried out with a Bruker LUMOS II FT-IR microscope (Bruker Optics GmbH, Ettlingen, Germany) with a germanium crystal in the 750–4000 cm^{-1} spectral region, with a resolution of 4 cm^{-1} and 64 scans. Preliminary point analysis was performed with a thermoelectric MCT detector (TE-MCT), while chemical imaging over a sampling area of approximately 50×50 μm^2 was performed with a liquid N_2-cooled 32×32 element Focal Plane Array (FPA) detector. Under these measurement conditions, a single spectrum in each FPA-FTIR image represents molecular information acquired from an area of proximately 1.5×1.5 μm^2 in the plane of the sample. The collected spectra were processed using OPUS 8.2 software.
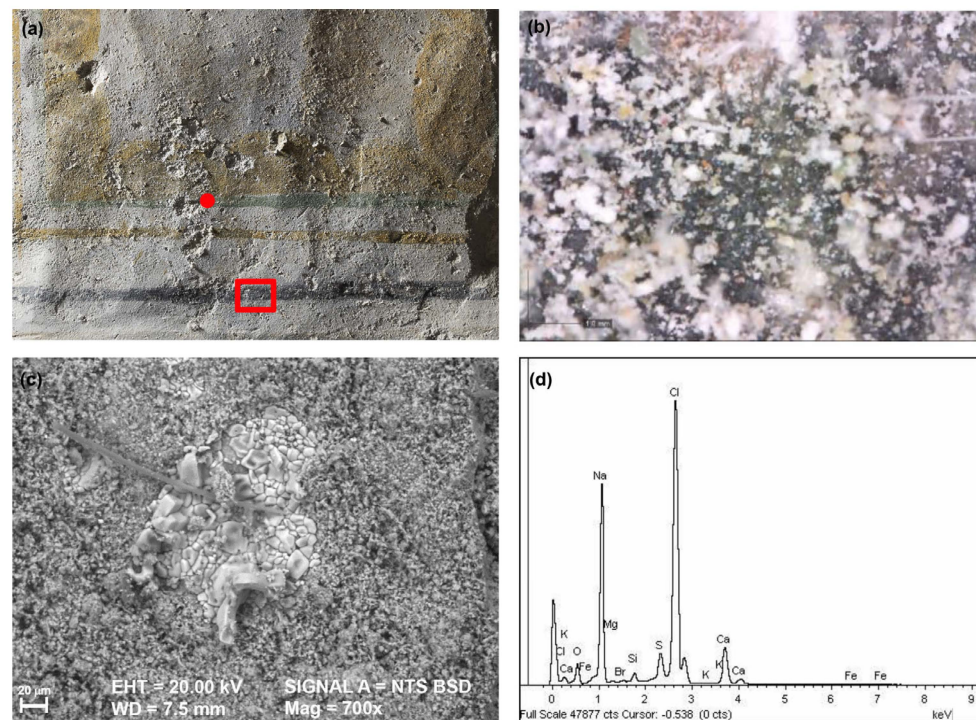
3. Results

A visual observation of the surface and the use of raking light photography provide a means of assessing the state of conservation of the surface and to highlight the guidelines imprinted on the surface with a chalk - line, especially where yellow and black decorations are visible.

The application of black lines appears to be imprecise, and some mistakes made by the painter are clearly visible. In certain areas of the surface, the drawing appears to have been executed hastily and with some degree of approximation (Figure S1).

3.1. Non-Invasive Techniques

Both sides of the surface exhibit irregularities, including extensive areas of spalling, flaking and powdering [20]. As previously stated in the introduction, the cippus was discovered during the construction of the new seaport in a burial site that was exposed to seawater. The combination of the conditions of the burial site, the porous nature of the stone used as support and the length of time spent underwater has resulted in seawater seeping into the object. Notwithstanding the restoration campaign [8], the process of water evaporation persists. This water, which contains salts, slowly evaporates over time, causing blistering phenomena on the stone surfaces [20–24] (Figure 2a).

Figure 2. (**a**) Raking light detail of flaking areas; (**b**) High magnification image (60×) of the area in the red square; (**c**) SEM image in BSE from the sample (red point) and (**d**) EDS analysis results of a point on recrystallized salt.

The presence of salts on the surface was also indicated by the SEM images and EDS spectra of the sample taken from the painted surface, where the characteristic structure of recrystallized salts is visible in different areas. The presence of recrystallized salts was also confirmed by the EDS analysis, with high counts for sodium (Na), chlorine (Cl) and sulfur (S) [25,26] (Figure 2c,d).

A spatial recognition of pigments was obtained through the MBI campaign, which was conducted on both painted surfaces to select areas to analyze with punctual techniques.

The ultraviolet-induced luminescence technique (UVL) is typically used to show the distribution of organic materials on a surface. However, in some cases, it can also reveal drawings or writings that are no longer visible to the naked eye, particularly when iron-based substances are present. UVL was performed on both sides of the object to highlight the presence of a residual drawing. Additionally, it was performed on the *tabella ansata* to identify any possible painted inscription. However, neither side exhibited any peculiar fluorescence and the *tabella* appeared to be completely blank (Figure S2). The images show the presence of a bluish luminescence, which is characteristic of calcium carbonate, and a slight yellow fluorescence distributed on the entire surface including the stone.

Reflected near-infrared photography (NIR) also enhanced small details of the drawing, such as the presence of leaves on the upper part of side A. In 2013, G. Gasperetti noted the presence of green traces in this area of the cippus that are no longer visible [8]. They were meant to be part of the leaves of a garland hanging from the upper part of the drawing, similar to the painted altar in the Civic Archaeological Museum in Milan [27].

Ultraviolet-reflected false color (UVFC) and near-infrared reflected photography out-performed the other techniques in showing the guidelines used for the geometric drawing and framing (Figure S3). Upon close examination, it was observed that the guidelines were engraved in the preparation and the visibility of the lines with the photographic techniques depended only on the type of pigment that had been trapped in the micro-rift created on the surface by the chalk-line.

Nevertheless, it was not possible to recognize the guidelines across the entire surface. For example, the aforementioned guidelines are absent on the frames of the *tabella*, where the lines appear to have been painted on a plane surface.

The ultraviolet-reflected false color (UVFC) and infrared reflected false color (IRFC) photography suggested the use of iron-based pigments for the yellow, dark yellow and green painting [28,29].

VIL was also performed on both sides to highlight the presence of Egyptian blue, but no evidence of this pigment was found [30].

Following the initial MBI analyses, several points were selected for further analysis using punctual techniques such as ER FT-IR, p-XRF and Raman spectroscopy. The ER FT-IR analysis was initially conducted on side A. However, poor-quality spectra were obtained due to the surface morphology and the presence of moisture, which discouraged further analysis on the other side.

However, the results from these techniques combined with the information obtained from the MBI provided a comprehensive characterization of the pigments.

A direct observation of the surface revealed the presence of a preparatory layer applied to the stone surface, formed by a visible aggregate consisting of different types of rocks. A comparison between the XRF spectra of the stone and the preparatory layer did not show any peculiar difference except for the increased counting for iron (Fe) content (Figure S4). The presence of the large amount of iron (Fe) observed in the preparation layer may be associated with the mineral embedded in the crushed stone.

The presence of sulfur (S) is likely related to the presence of degradation products, such as sulfates, emerging on the surface.

The white/grey areas on both sides of the cippus appeared to be the most extensive, especially on side A. However, upon closer observation, the distinction between the white/grey layer and the background was difficult to discern. It is plausible to suggest that the white areas may have been obtained using calcite as the background, precluding the recognition of the material.

Some attempts were made to characterize the material responsible for this chromatic difference, but the Raman spectra and XRF spectra did not show any differences compared to those of the background. The Raman spectrum of the bluish/greyish areas showed peaks for calcite (1086 cm^{-1}) and gypsum (1008 cm^{-1}) [31], whereas the XRF spectra compared with the preparation layer differed only for counts related to chlorine. The presence of chlorine can be easily related to the presence of chlorides, and thus to the conservation history of the object and its underwater burial in the seaport area (Figure S5).

Furthermore, the presence of a considerable quantity of calcite was detected in the investigated volume contributed to a flattening of all the other peaks making the material identification more challenging using Raman techniques.

Despite this consideration, the black areas exhibited two broader bands at 1596 and 1320 cm^{-1}, indicative of the presence of amorphous carbon, such as charcoal [32–35] (Figure 3a). The XRF measurements excluded the presence of manganese-based black pigments.

Regarding the yellow areas, p-XRF showed the presence of iron (Fe) and traces of manganese (Mn) and titanium (Ti). A comparison of the Raman spectrum with the goethite spectrum obtained from the RRUFF mineral database [31] showed a peak at 389 cm^{-1} and a small shoulder at 302 cm^{-1}, confirming the presence of a yellow ochre [36] (Figure 3b).

Traces of elements such as manganese (Mn) and titanium (Ti) are not uncommon in the pigment category known as yellow ochre [37].

Some points on the yellow area, in this case, on side B of the cippus, showed the presence of traces of lead (Pb) and zinc (Zn) in addition to titanium (Ti), suggesting the use of another type of yellow ochre containing impurities such as zinc (Zn) (Figure S6) [38–40]. The presence of lead (Pb), which was always detected in traces in other few analyzed points, suggests the presence of retouches executed in ancient times. The precise period of these retouches is uncertain, although it can be stated with certainty that they are not

contemporary with the original painting, which was probably made when the plaster was still wet [8].
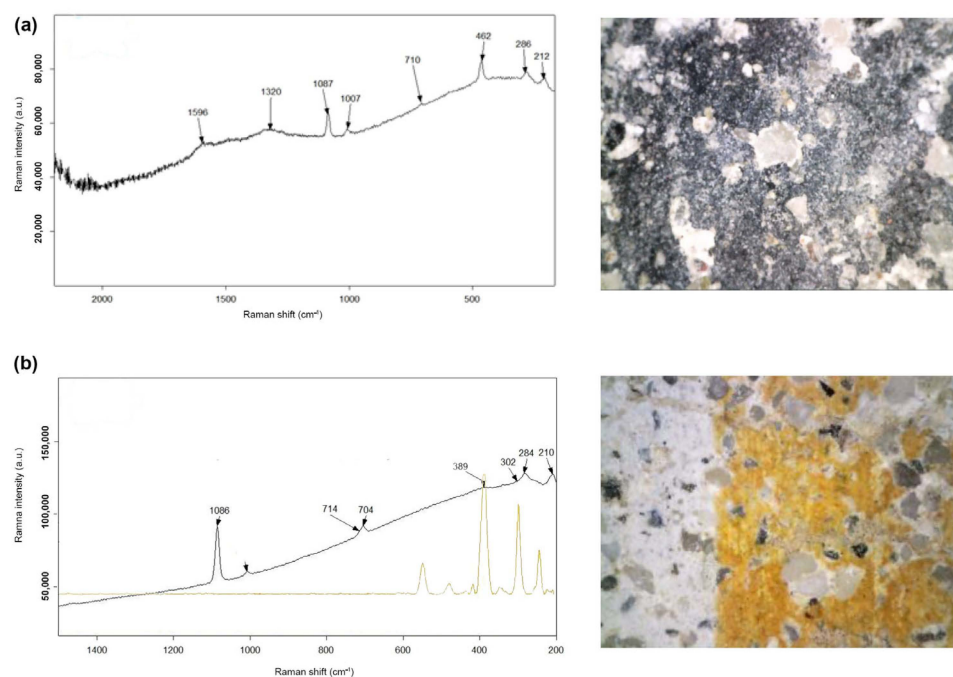
Figure 3. (a) Raman spectrum of point corresponding to (a) a black area and (b) a yellow area, respectively. On the right, the optical microscopic details of the points (60×). In (b) Raman spectrum of yellow area, in black, and goethite reference spectrum in yellow (RRUFF mineral database).

From an analytical point of view, the dark yellow areas showed a comparable composition to that observed in the yellow ones. A comparison between the XRF spectra showed differences only in the counts for chlorine (Cl) and iron (Fe). The increased amount of iron (Fe) can be explained by the thickness of the paint in those areas and by the presence of a mixture with a green pigment, probably an iron-based pigment, as suggested by the observation under the microscope (Figure S6).

The p-XRF spectrum also showed the presence of high counts for chlorine (Cl). This light, soluble element could be detected only on the surface of the material, indicating that it may be a residual of a chlorine-based mineral resulting from the evaporation of seawater (halite, sylvite and carnallite) [41,42] or from aerosol deposition [22]. Furthermore, the hypothesis was confirmed by the presence of traces of bromine (Br), which is commonly found in seawater [43].

The preliminary analyses conducted with imaging techniques narrowed the possible class for the material for the green painting. The VIL analysis of the green areas excluded the use of Egyptian blue to obtain the green color, while p-XRF confirmed the absence of any other copper-based green pigment (Figure 4a,b).

The analysis of both green areas on the two sides showed the presence of high counts for iron (Fe) (Figure 4a), suggesting the use of an iron-based earth pigment. The Raman spectra did not show peaks associated with glauconite or celadonite, the main constituents of the green earth class, but rather appeared to be another type of green phyllosilicate [44]. The spectra acquired in the green areas (i.e., points 8 and 10) showed the presence of peaks at 416 and 383 cm^{-1} that can be attributed to another phyllosilicate, such as chlorite (Figure 4c).

All the identified pigments on the cippus are consistent with those typically found on similar painted objects from the same period.
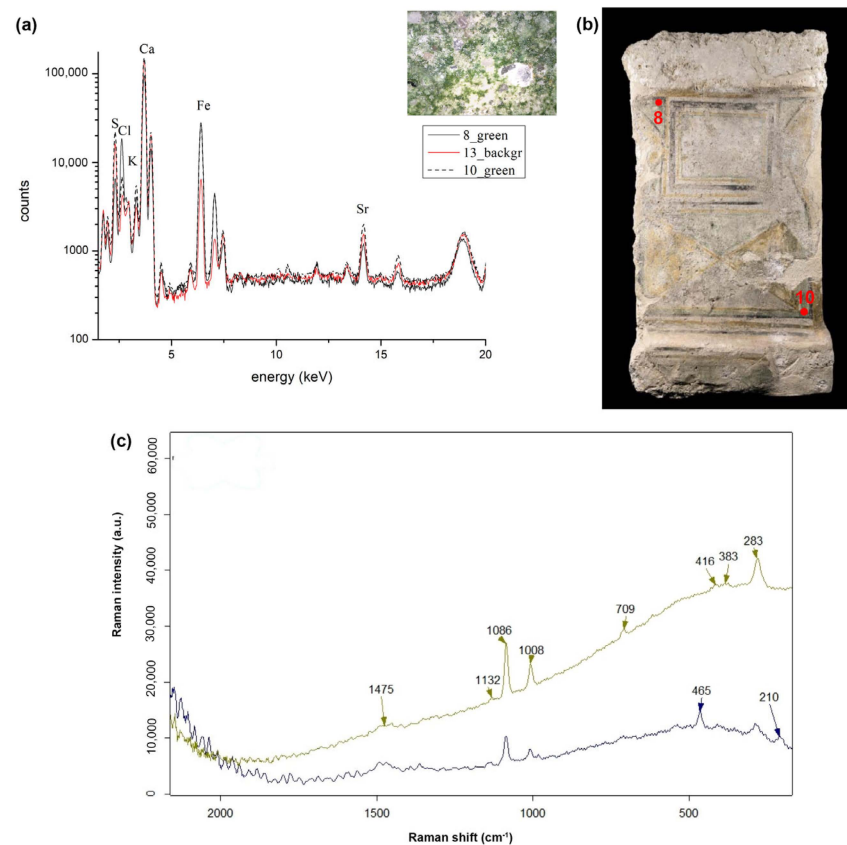
Figure 4. (**a**) p-XRF spectra of point 8 in black, point 10 in dotted black and the reference background in red; (**b**) the locations of measured points 8 and 10 are shown (**c**) Raman spectra of green earth pigment at point 8 (in green) and point 10 (in gray).

3.2. Micro-Destructive Techniques

Micro-invasive techniques were used to study, in detail, the petrographic and mineralogical composition of the stone used as the base, the preparation layer, as well as the aggregates that were mixed into the mortar.

In addition, an in-depth analysis of the green pigment was conducted with the objective of identifying its mineral composition.

Three samples were taken in order to better characterize the green pigment and to try to gather information about the provenance of the material used as the stone and preparation layer.

The mineralogical composition of the stone is characterized by calcite, while in the mortar sample, calcite and quartz are the most abundant phases, with feldspar, aragonite and gypsum present in relatively low amounts.

The petrographic observations indicated that the stone sample is a carbonatic rock, specifically a grainstone according to the Dunham classification [45], characterized by the presence of bioclastic fragments (i.e., algal thallus, oolithic structures and coralline algae) in a sparry calcite (Figure 5a,b). The rock sample shows intergranular porosity (~3%) with irregularly shaped pores. The mortar is composed of an aerial-lime binder with a micritic texture; the aggregate, which was poorly distributed, contains quartz crystals, magmatic rock fragments with a microcrystalline texture (probably rhyolites), biotite crystals, acicular feldspars and oxides, a single foraminifer, a single calcite fragment and a fragment of calcarenite (Figure 5c,d). The aggregate has a predominantly sub-rounded shape and shows a bimodal grain size distribution consisting of a fine fraction (size < 250 μm) and rare grains with a size > 500 μm, with the maximum grain size being 1.3 mm. The binder-to-aggregate ratio is 2/1.
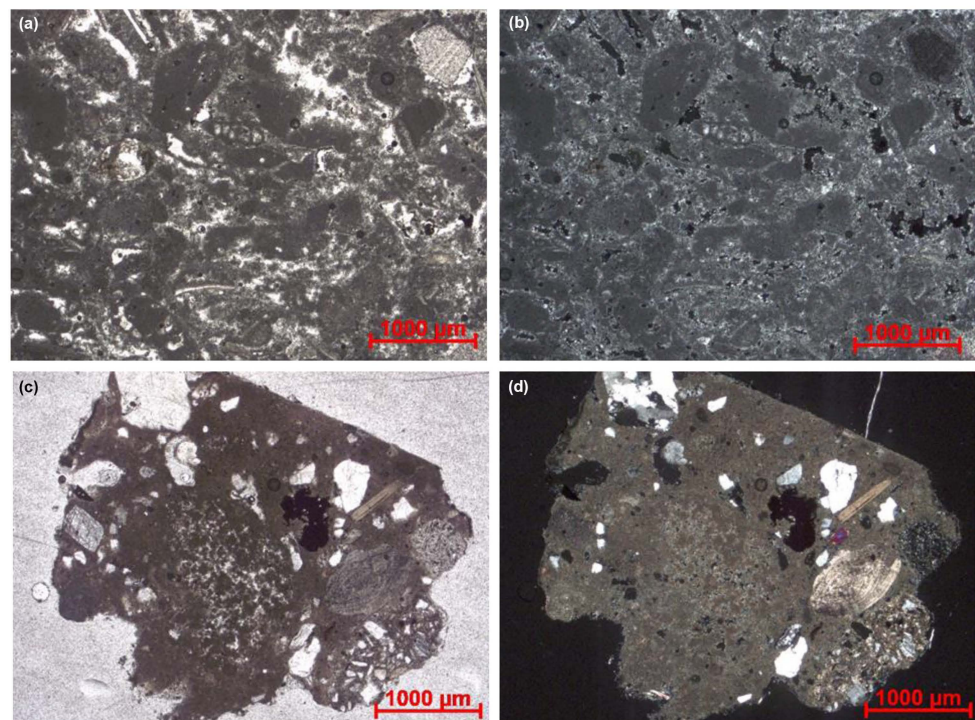
Figure 5. Microphotographs of thin sections of the carbonate rock of the cippus (**a**,**b**) and of the mortar covering the cippus (**c**,**d**) (using a polarized light microscope): (**a**,**c**) parallel nicols; (**b**,**d**) crossed nicols.

The analysis conducted permitted the identification of all the geomaterials, both the rock body and the mortar raw materials, which are consistent with the geological formations outcropping near Porto Torres. Figure 6 presents a detail of the geological map of Porto Torres and its surrounding area.

Porto Torres is located in a half-graben and is characterized by Miocene deposits, namely the Mores Formation. This presents two lithofacies, a littoral carbonate deposit of calcarenites and calcitic sandstones (11a, also named "Calcari di Mores-Logudoro") and a marine deposit composed of sandstones and conglomerates with carbonatic cement, marls and marly sandstones, with fossils of planktonic foraminifers, mollusks, echinoids and corals (11b). All these sediments outcrop extensively around the town, with their ages ranging from the Upper Burdigalian (~17 Mya) for lithofacies 11a to the Upper Budigalian–Middle-Upper Langhian (~14–17 Mya) for lithofacies 11b.

Fragments of both lithofacies are present as aggregate within the analyzed mortar sample. Fossils of foraminifera and algal tallus from 11b, along with the fragments of sub-rounded quartz, could have originated from both lithofacies, while the sparitic carbonate fragments, such as the calcarenite fragment, could come from 11a. With regard to the aggregate with a magmatic nature, a resemblance was found with the Candelazzos unit (18), an outcropping a few kilometers west of Porto Torres. The unit consists of ignimbritic unwelded deposits of rhyolitic/rhyo-dacitic pyroclasts deposited during the Burdigalian phase of the explosive volcanism in northern Sardinia.

The presence of fossils (including a clearly Mesozoic ammonite) was very useful in establishing the origin of the initial carbonate rock (Figure 7). This characteristic suggested the Jurassic bioclastic limestone of Mount Alvaro (a few kilometers south-west of the town of Porto Torres) as the possible origin of the lithic material employed in the construction of the cippus.
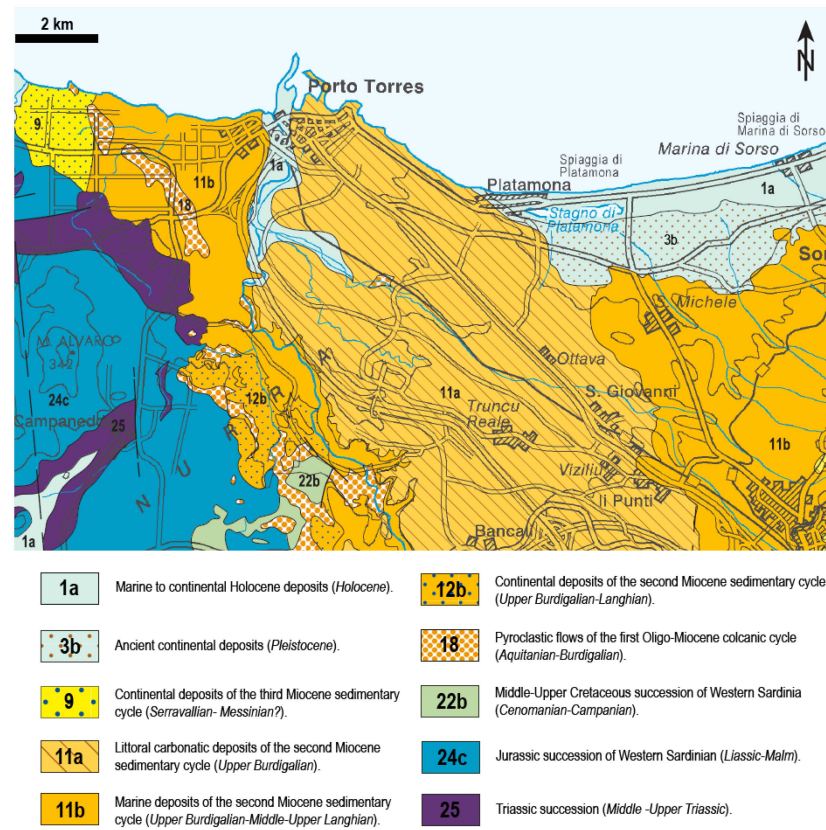
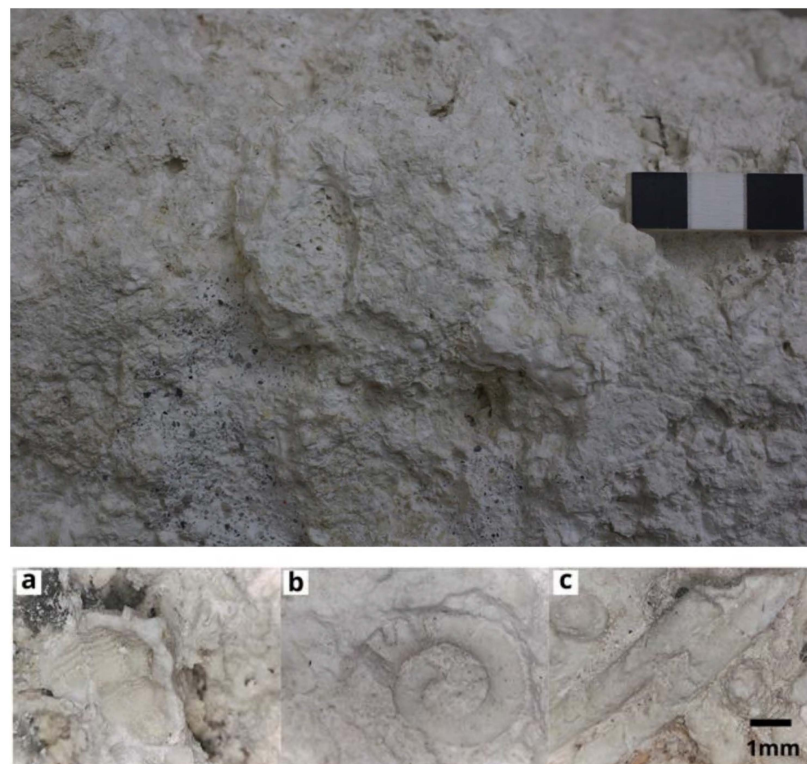**Figure 6.** Geological map of Porto Torres and its surrounding area. Modified from [46].

Figure 7. Macro-photo of carbonate rock of the cippus. Various fossils were observed in the carbonatic rock of the cippus: (**a**) gastropods; (**b**) ammonites; (**c**) algae tallus.

The green sample was analyzed by SEM-EDS and FPA-ATR FT-IR spectroscopy, with the aim of obtaining a more detailed characterization of the mineralogical phase. The literature in the geological field reveals a clear distinction between the two main minerals that constitute what is commonly referred to as "green earth": celadonite and glauconite. However, the mineralogical composition of the latter does not always correspond with what was sold in the past as pigment. This results in a significant challenge in characterizing the material, which is further complicated by the presence of other compounds [47].

A microsample was taken from the edge of a lacuna in order to minimize the visual impact on the object. The sample was analyzed by SEM without being embedded in resin, with the fragment placed directly on the stub. The sample showed a highly deteriorated surface, with the presence of areas with crystalline aggregates, mainly comprising salt outcrops (Figure 8). The micro-analysis showed the presence of calcium (Ca) and silicon (Si) as the main constituents and iron (Fe), potassium (K), aluminum (Al) and magnesium (Mg) as secondary elements.
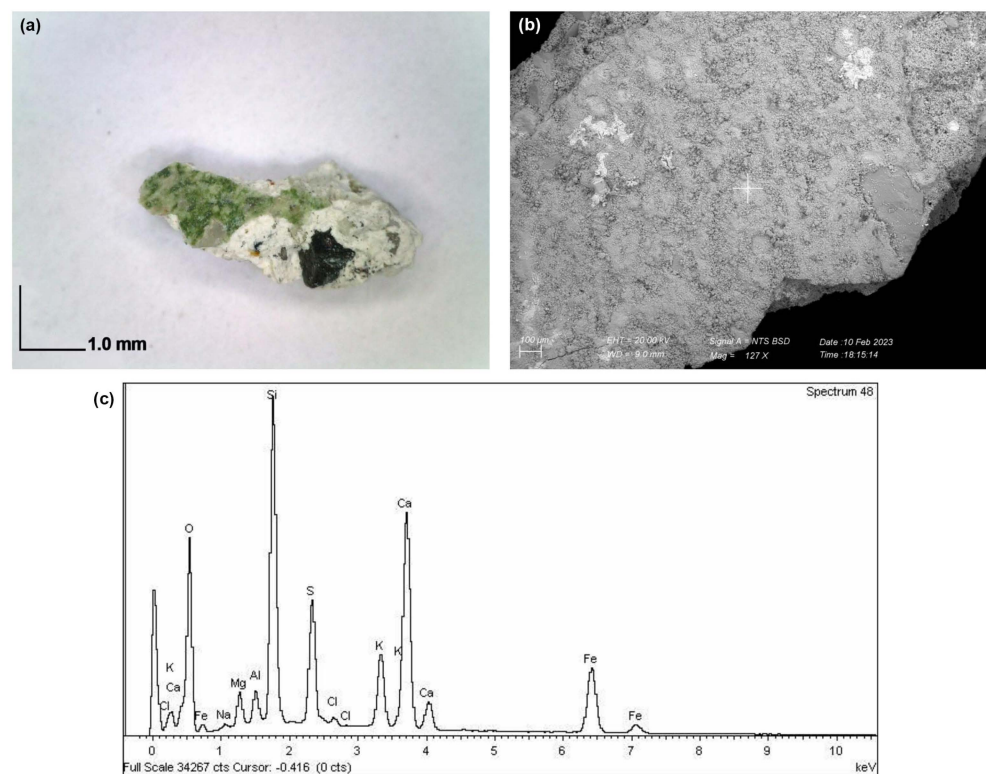
Figure 8. Fragment analyzed by SEM−EDS. (**a**) Optical microscope image at 50×; (**b**) backscattered details at 127×; and (**c**) EDS analysis results.

The surface morphology does not permit the identification of any potential mineralogical structure due to the sample's condition (since it is in a powdery form and incoherent). The mapping of a portion of the sample revealed the presence of a significant area of recrystallized salt, while silica (Si), magnesium (Mg), aluminum (Al) and iron (Fe) were observed to be distributed throughout the entire surface, accompanied by sulfur (S), which is probably associated with the presence of sulfates, due to the conservation condition. FT-IR micro-ATR spectroscopy of the same microsample revealed the presence of intense bands for gypsum (νOH at 3545 and 3400 cm^{-1}; δOH at 1684 and 1621 cm^{-1}; νSO4 at 1117 cm^{-1}) [48] and calcite ($\nu_1 + \nu_{4\text{sym}}CO_3$ at 1800, $\nu^{3\text{asym}}$CO$_3$ at 1412, $\nu_{2\text{asym}}$CO$_3$ at 871 cm^{-1}) [49], as well as bands suggestive of silicates (945–1037 cm^{-1}), whose interpretation is complex due to their low intensity and interference from the support (Figure 9a). However, the chemical imaging at a high lateral resolution, obtained through further investigation with FT-IR FPA-ATR microscopy, allowed for the detection of a few traces of a

silicate whose spectral profile is compatible with that of celadonite, as suggested by the well-resolved ν(Si-O) bands (1115, 1071 and 974 cm^{-1}; Figure 9b) [44,50]. However, the water vapor vibrations in the 3000–3600 cm^{-1} range may prevent the detection of the other diagnostic bands for celadonite at 3534, 3555 and 3601 cm^{-1} (νOH), while the δ(SiO) bands below 800 cm^{-1} fall outside the instrument's range of acquisition.
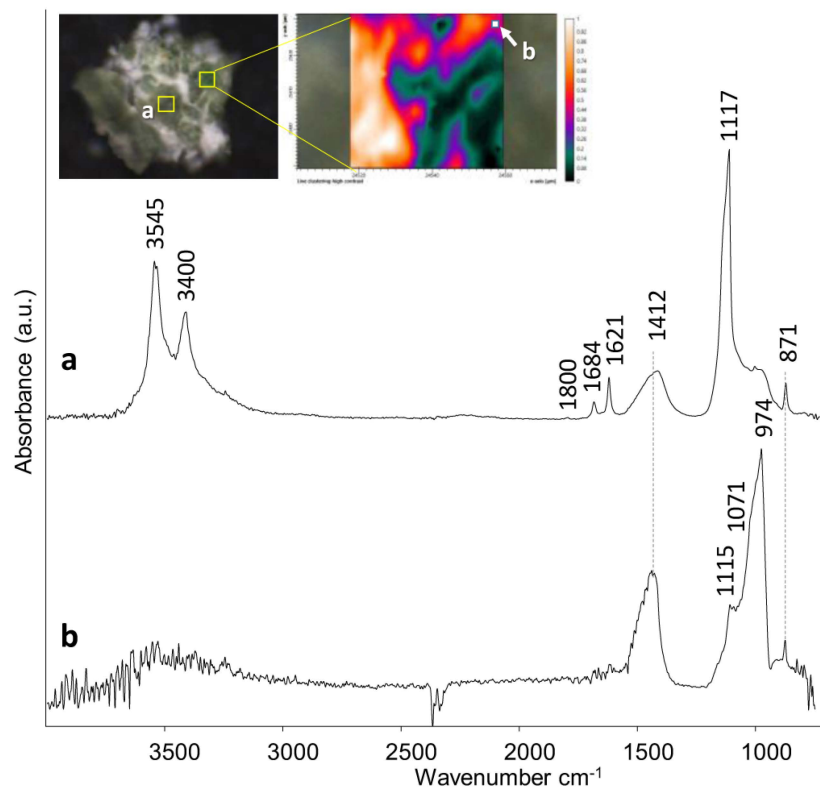
Figure 9. (**a**) FT-IR micro-ATR spectrum obtained from the green sample using point analysis with a TE-MCT detector and (**b**) FT-IR FPA-ATR spectrum extracted from the chemical map shown above. The arrow indicates the position of the spectrum.

4. Discussion

The UVL images suggest the use of a carbonate binder, a technique analogous to that used in fresco painting. The results of the analyses demonstrated that for the decoration were used cheap pigments, such as yellow ochres, a green iron-based phyllosilicate and a carbon black pigment, which were used in the wall paintings during the Roman period and are consistent with the pigments allowed by fresco techniques [51,52].

The nature of the white/grey pigment remains uncertain. In particular, these areas are the most severely deteriorated, with the paint layers revealing the underlying preparation layer. It can be reasonably deduced from the analysis and the technique used in creating the painting layers that calcium carbonate may have been employed. Although it is well documented that gypsum was used as a pigment during the Roman period, due to the poor state of conservation of the artefact and the extensive presence of gypsum on the entire surface, we are inclined to attribute the substance to a secondary product resulting from the decay of the carbonate stone.

For the green pigment, it would be of interest to ascertain whether the extensive use of green in paintings in Turris Libisonis, such as on the painted plaster fragments preserved in the Antiquarium Turritano itself, could be related to the use of a specific green local earth pigment. The FT-IR analyses conducted on the microsamples only detected minimal traces of a silicate compatible with celadonite, and the evidence was not sufficient to attribute the observed color to this mineral, suggesting an interesting sourcing for

this pigment. Nevertheless, the co-occurrence of silicate (Si) with iron (Fe) in the p-XRF and SEM results of the green areas, along with the Raman peaks, suggests the use of a phyllosilicate. Nevertheless, the wide range of minerals within this class precludes a definitive identification.

There was no specific pattern for the presence of lead at the measured points and it was not linked to a specific color; thus, in the past, the painting was probably refreshed and retouched with a pigment mixed with a small amount of white lead or another hypothesis is that a mixture of yellow ochre and white lead was used to paint some areas after the first layer on the wet plaster. The small amount of lead detectable with p-XRF can be connected to the entity of the areas interested by this second layer.

For the painting, one of the main comparisons for this object is an altar from Milan, an object linked to the votive sphere, with deities on the four sides and garlands in the upper part of the representation [53]. In this case, the images were also depicted on a preparatory layer with the use of ochres and a black-colored pigment, according to the literature [27]. Other examples of painted altars are known from Spain [54], but also from Pozzuoli [55] and the Vesuvian cities (for example, Terzigno, villa 6) [56] and, in a later funerary context with a wide group of painted *arae*, from Tunisia [57]. However, the cippus of Turris Libisonis is not, as far as we know, strictly comparable with other Roman objects, and it is an original creation of the Roman colony made with local materials (stone and pigments).

5. Conclusions

In this paper, a complete characterization of a cippus from Turris Libisonis, exhibited in the Antiquarium Turritano, is presented using non-invasive techniques supported by micro-invasive techniques. This approach presents a comprehensive study of the artifact and its conservation status, providing valuable insights for archaeologists and conservators and represents a significant advancement in the study of Roman Sardinia.

The non-invasive protocol used for the characterization of the pigments on the cippus allowed us to gather information about the materials, the technique used, and the conservation status of the artefact.

The results from some of the microsamples allowed us to clarify the provenance and the materials used to create the cippus. Regarding the raw materials used for the painting, no traces of Egyptian blue were found, nor was it mixed with other pigments for the green and grey colors. The use of a mineral belonging to the green earth group to create the green decorations is a precise choice of the painter since the trading of Egyptian blue in Turris Libisonis was proven by the discovery of a blue pallet, which is currently preserved in the Antiquarium Turritano.

Among the questions raised by archaeologists was whether there is residual text surviving on the *tabella ansata*. The MBI results showed no traces of painted text on it; despite this, MBI provided other interesting data. For example, on the white background of side A, a possible garland was enhanced in the upper part, thus giving new data about the original drawing on the cippus.

Moreover, the raking light and other MBI techniques allowed us to observe the guidelines imprinted with a chalk-line for the painting, which were still visible on the surface, especially for yellow and black lines. The painting of the black lines was not carefully applied, and some mistakes made by the painter are still visible. The drawing seems to have been done quickly and with a certain degree of approximation. However, it does not appear to be an unfinished drawing, and the absence of text in the tabula ansata probably does not support this hypothesis.

The investigated cippus is not the only colored object from Turris Libisonis and wider research on polychromy is necessary in order to understand the colors and pigments used in this Roman colony and their context.

This paper on a painted object from the seaport of Porto Torres is just a first step in research on the colors of Roman Sardinia, which is worth carrying out for a deeper knowledge of the original aspect of the sculptures—either local or imported—in this region.

References

1. Boninu, A. Turris Libisonis Colonia Iulia. In *La Sardegna Romana e Altomedievale. Storia e Materali*; Angiolillo, S., Martorelli, R., Giuman, M., Corda, A.M., Artizzu, D., Eds.; Regione Autonoma della Sardegna: Cagliari, Italy, 2017; pp. 149–158.
2. Plinius the Elder. *Naturalis Historia*, III, 7, 85. Available online: https://penelope.uchicago.edu/Thayer/l/roman/texts/pliny_the_elder/3*.html (accessed on 12 October 2024).
3. Zucca, R. Colonia Iulia Turris Libisonis. In *Storia della Sardegna Antica*; Mastino, A., Ed.; Edizioni Il Maestrale: Nuoro, Italy, 2005; pp. 273–283.
4. Mastino, A. Popolazioni e classi sociali a Turris Libisonis: I legami con Ostia. In *Turris Libisonis Colonia Iulia*; Boninu, A., LeGlay, M., Mastino, A., Eds.; Edizioni Gallizzi: Sassari, Italy, 1984; pp. 37–96.
5. Mastino, A.; Spanu, P.G.; Zucca, R.; Merci, M.S. *Mercati e Scambi Marittimi della Sardegna Antica*; Carrocci Editore: Rome, Italy, 2005.
6. Canu, N. Colonia Iulia Turris Libisonis. In *Il Tempo dei Romani. La Sardegna dal III Secolo A.C. al V Secolo D.C.*; Carboni, R., Giuman, M., Corda, A.M., Eds.; Ilisso: Nuoro, Italy, 2021; pp. 88–99.
7. Giuliani, S. L'Antiquarium Turritano e l'area archeologica di Porto Torres. Alla scoperta della Sardegna romana. In *Italia. Musei da Scoprire. Sardegna*; Toniolo, L., Ed.; L'Erma di Bretschneider: Rome, Italy, 2022; pp. 37–49.
8. Gasperetti, G. Reperti dal porto commerciale di Porto Torres. In *Memorie dal Sottosuolo. Scoperte Archeologiche nella Sardegna Centro—Settentrionale. Catalogo della Mostra. Sassari, Museo Nazionale "Giovanni Antonio Sanna", Padiglione Clemente, Febbraio 2011—Aprile 2013*; Usai, L., Ed.; Scuola Sarda Editrice: Quartucciu, CA, USA, 2013; pp. 267–272.
9. Boninu, A. Terme Maetzke—Terme Centrali—Via Ponte Romano. In *Marmore Fluctus. Reperti Marmorei e Indagini Archeologiche a Turris Libisonis*; Colombi, R., Pandolfi, A., Eds.; Istituti Editoriali e Poligrafici Internazionali: Rome, Italy, 2004; pp. 12–14.
10. Grasso, F. Parete con nature morte. In *La Pittura Pompeiana*; Sampaolo, V., Ed.; Electa: Naples, Italy, 2009; pp. 372–373.
11. Candida, B. *Altari e Cippi nel Museo Nazionale Romano*; Bretschneider Giorgio: Rome, Italy, 1979; Volume 10.
12. Zevi, F. Base di statua di Nerva. In *Museo Archeologico dei Campi Flegrei. Catalogo Generale, Liternum, Baia, Miseno*; Miniero, P., Zevi, F., Eds.; Electa Napoli: Naples, Italy, 2008; Volume III, p. 221.
13. Iannaccone, R.; Bracci, S.; Cantisani, E.; Mazzei, B. An integrated multimethodological approach for characterizing the materials and pigments on a sarcophagus in St. Mark, Marcellian and Damasus catacombs. *Appl. Phys. A* **2015**, *121*, 1235–1242. [CrossRef]
14. Magrini, D.; Bracci, S.; Bartolozzi, G.; Iannaccone, R.; Lenzi, S.; Liverani, P. Revealing mithras' color with the icvbc mobile lab in the museum. *Heritage* **2019**, *2*, 2160–2170. [CrossRef]
15. Dyer, J.; Verri, G.; Cupitt, J. Multispectral Imaging in Reflectance and Photo-Induced Luminescence Modes: A User Manual. 2013. Available online: https://www.britishmuseum.org/pdf/charisma-multispectral-imaging-manual-2013.pdf (accessed on 14 September 2024).

16. Svoboda, M.; Cartwright, C.R. *Mummy Portraits of Roman Egypt*; J. Paul Getty Museum: Los Angeles, CA, USA, 2020.

17. Miliani, C.; Rosi, F.; Daveri, A.; Brunetti, B.G. Reflection infrared spectroscopy for the non-invasive in situ study of artists' pigments. *Appl. Phys. A Mater. Sci. Process.* **2012**, *106*, 295–307. [CrossRef]

18. Conti, C.; Botteon, A.; Bertasa, M.; Colombo, C.; Realini, M.; Sali, D. Portable Sequentially Shifted Excitation Raman spectroscopy as an innovative tool for: In situ chemical interrogation of painted surfaces. *Analyst* **2016**, *141*, 4599–4607. [CrossRef]

19. Moioli, P.; Seccaroni, C. Analysis of Art Objects Using a Portable X-ray Fluorescence Spectrometer. *X-ray Spectrom. Int. J.* **2000**, *29*, 48–52. [CrossRef]

20. Cartwright, T.A.; Bourguignon, E.; Bromblet, P.; Cassar, J.; Charola, A.E.; De Witte, E.; Delgado-Rodrigues, J.; Fassina, V.; Fitzner, B.; Fortier, L.; et al. *ICOMOS-ISCS: Illustrated Glossary on Stone Deterioration Patterns*; International Council of Monuments and Sites: Paris, France, 2011; Volume 1.

21. Flatt, R.J.; Aly Mohamed, N.; Caruso, F.; Derluyn, H.; Desarnaud, J.; Lubelli, B.; Espinosa-Marzal, R.M.; Pel, L.; Rodriguez-Navarro, C.; Scherer, G.W.; et al. Predicting salt damage in practice: A theoretical insight into laboratory tests. *RILEM Tech. Lett.* **2017**, *2*, 108–118. [CrossRef]

22. Zezza, F.; Macrì, F. Marine aerosol and stone decay. *Sci. Total Environ.* **1995**, *167*, 123–143. [CrossRef]

23. La Iglesia, A.; del Cura, M.A.G.; Ordoñez, S. The physicochemical weathering of monumental dolostones, granites and limestones; dimension stones of the Cathedral of Toledo (Spain). *Sci. Total Environ.* **1994**, *152*, 179–188. [CrossRef]

24. Pearson, C. *Conservation of Marine Archaeological Objects*; Elsiever: Oxford, UK, 2014.

25. Benavente, D.; del Cura, M.A.G.; García-Guinea, J.; Sánchez-Moral, S.; Ordóñez, S. Role of pore structure in salt crystallisation in unsaturated porous stone. *J. Cryst. Growth* **2004**, *260*, 532–544. [CrossRef]

26. da Fonseca, B.S.; Pinto, A.P.F.; Rucha, M.; Alves, M.M.; Montemor, M.F. Damaging effects of salt crystallization on a porous limestone after consolidation treatments. *Constr. Build. Mater.* **2023**, *374*, 130967. [CrossRef]

27. Chiesa, G.S. Ara Dipinta. In *Romana Pictura. La Pittura Romana dalle Origini all'età Bizantina, Rimini, 28 Marzo–30 Agosto 1998*; Donati, A., Ed.; Electa Milano: Milan, Italy, 1998; Chapter 25; pp. 277–278.

28. Aldrovandi, A.; Picollo, M. *Metodi di Documentazione e Indagini non Invasive sui Dipinti*; Il Prato: Saonara, Italy, 2001.

29. Bevilacqua, N.; Borgioli, L.; Gracia, I.A. *I Pigmenti nell'arte: Dalla Preistoria alla Rivoluzione Industriale*; Il Prato: Saonara, Italy, 2010.

30. Accorsi, G.; Verri, G.; Bolognesi, M.; Armaroli, N.; Clementi, C.; Miliani, C.; Romani, A. The exceptional near-infrared luminescence properties of cuprorivaite (Egyptian blue). *Chem. Commun.* **2009**, *23*, 3392–3394. [CrossRef]

31. Lafuente, B.; Downs, R.T.; Yang, H.; Stone, N. The power of databases: The RRUFF project. In *Highlights in Mineralogical Crystallography*; Armbruster, T., Danisi, R.M., Eds.; W. De Gruyter: Berlin, Germany, 2015; pp. 1–30. [CrossRef]

32. Tuinstra, F.; Koenig, J.L. Raman Spectrum of Graphite. *J. Chem. Phys.* **1970**, *53*, 1126–1130. [CrossRef]

33. Beny-Bassez, C.; Rouzaud, J.N. Characterization of carbonaceous materials by correlated electron and optical microscopy and Raman microspectroscopy. *Scanning Electron Microsc.* **1985**, *1*, 119–132.

34. Beyssac, O.; Goffé, B.; Petitet, J.P.; Froigneux, E.; Moreau, M.; Rouzaud, J.N. On the characterization of disordered and heterogeneous carbonaceous materials by Raman spectroscopy. *Spectrochim. Acta A Mol. Biomol. Spectrosc.* **2003**, *59*, 2267–2276. [CrossRef]

35. Lluveras-Tenorio, A.; Spepi, A.; Pieraccioni, M.; Legnaioli, S.; Lorenzetti, G.; Palleschi, V.; Vendrell, M.; Colombini, M.P.; Tinè, M.R.; Duce, C.; et al. A multi-analytical characterization of artists' carbon-based black pigments. *J. Therm. Anal. Calorim.* **2019**, *138*, 3287–3299. [CrossRef]

36. Froment, F.; Tournié, A.; Colomban, P. Raman identification of natural red to yellow pigments: Ochre and iron-containing ores. *J. Raman Spectrosc.* **2008**, *39*, 560–568. [CrossRef]

37. Eastaugh, N.; Walsh, V.; Chaplin, T.; Siddal, R. *Pigment Compendium. A Dictionary and Optical Microscopy of Historical Pigments*; Routledge: London, UK, 2013; Volume 53. [CrossRef]

38. Cornell, R.; Schwertmann, U. The Iron Oxides: Structure, Properties, Reactions, Occurrences, and Uses. 2003. Available online: https://www.degruyter.com/document/doi/10.1515/CORRREV.1997.15.3-4.533/pdf?licenseType=restricted (accessed on 8 October 2024).

39. Cruz-Jiménez, G.; Loredo-Portales, R.; Del Rio-Salas, R.; Moreno-Rodríguez, V.; Castillo-Michel, H.; Ramiro-Bautista, L.R.; Aquilanti, G.; De La Rosa-Álvarez, M.G.; Rocha-Amador, D.O. Multi-synchrotron techniques to constrain mobility and speciation of Zn associated with historical mine tailings. *Chem. Geol.* **2020**, *558*, 119866. [CrossRef]

40. Jerzykowska, I.; Majzlan, J.; Michalik, M.; Göttlicher, J.; Steininger, R.; Błachowski, A.; Ruebenbauer, K. Mineralogy and speciation of Zn and As in Fe-oxide-clay aggregates in the mining waste at the MVT Zn–Pb deposits near Olkusz, Poland. *Geochemistry* **2014**, *74*, 393–406. [CrossRef]

41. Johnson, J. Soluble Salts and Deterioration of Archeological Materials. 1998. Available online: https://repository.si.edu/bitstream/handle/10088/56540/ConserveOGram06-05.pdf (accessed on 10 April 2024).

42. Steiger, M.; Charola, A.E.; Sterflinger, K. Weathering and deterioration. In *Stone in Architecture: Properties, Durability*; Springer Science and Business Media: New York, NY, USA, 2011; pp. 227–316. [CrossRef]

43. Torfs, K.; Van Grieken, R. Chemical relations between atmospheric aerosols, deposition and stone decay layers on historic buildings at the Mediterranean coast. *Atmos. Environ.* **1997**, *31*, 2179–2192. [CrossRef]

44. Ospitali, F.; Bersani, D.; Di Lonardo, G.; Lottici, P.P. 'Green earths': Vibrational and elemental characterization of glauconites, celadonites and historical pigments. *J. Raman Spectrosc.* **2008**, *39*, 1066–1073. [CrossRef]

45. Dunham, R.J. Classification of Carbonate Rocks According to Depositional Textures. 1962, pp. 108–121. Available online: https://archives.datapages.com/data/specpubs/carbona2/data/a038/a038/0001/0100/0108.htm (accessed on 13 August 2024).

46. Carmignani, L.; Oggiano, G.; Funedda, A.; Conti, P.; Pasci, S. The geological map of Sardinia (Italy) at 1:250,000 scale. *J. Maps* **2015**, *12*, 826–835. [CrossRef]

47. Fanost, A.; Gimat, A.; de Viguerie, L.; Martinetto, P.; Giot, A.C.; Clémancey, M.; Blondin, G.; Gaslain, F.; Glanville, H.; Walter, P.; et al. Revisiting the identification of commercial and historical green earth pigments. *Colloids Surf. A Physicochem. Eng. Asp.* **2020**, *584*, 124035. [CrossRef]

48. Knittle, E.; Phillips, W.; Williams, Q. An infrared and Raman spectroscopic study of gypsum at high pressures. *Phys. Chem. Min.* **2001**, *28*, 630–640. [CrossRef]

49. Rodriguez-Blanco, J.D.; Shaw, S.; Benning, L.G. The kinetics and mechanisms of amorphous calcium carbonate (ACC) crystallization to calcite, viavaterite. *Nanoscale* **2011**, *3*, 265–271. [CrossRef]

50. Singh, P.; Banerjee, S.; Choudhury, T.R.; Bhattacharya, S.; Pande, K. Distinguishing celadonite from glauconite for environmental interpretations: A review. *J. Palaeogeogr.* **2023**, *12*, 179–194. [CrossRef]

51. Aliatis, I.; Bersani, D.; Campani, E.; Casoli, A.; Lottici, P.P.; Mantovan, S.; Marino, I.G.; Ospitali, F. Green pigments of the Pompeian artists' palette. *Spectrochim. Acta Part A Mol. Biomol. Spectrosc.* **2009**, *73*, 532–538. [CrossRef]

52. Mateos, L.D.; Cosano, D.; Esquivel, D.; Osuna, S.; Jiménez-Sanchidrián, C.; Ruiz, J.R. Use of Raman microspectroscopy to characterize wallpaintings in Cerro de las Cabezas and the Roman villa of Priego de Cordoba (Spain). *Vib. Spectrosc.* **2018**, *96*, 143–149. [CrossRef]

53. Caporusso, D.; Donati, M.T.; Masseroli, S.; Tibiletti, T.; Gerli, V. *Civico Museo Archeologico. Sezione Milano Antica V Secolo A.C.—V Secolo D.C.*; Edizione Et: Milan, Italy, 2016.

54. Prieto, F.J.N. Una ara pintada de ampurias dedicada a Esculapio. *Ampurias* **1971**, *72*, 385–390. Available online: https://www.raco.cat/index.php/Empuries/article/download/117168/287812 (accessed on 3 June 2024).

55. Proietti, L.M. Il Larario ubicato all'incrocio tra il decumano di Via Duomo e il cardine di Via San Proclo. In *Nova antiqua Phlegraea. Nuovi Tesori Archeologici dai Campi Flegrei*; Gialanella, C., Ed.; Electa: Naples, Italy, 2000; pp. 39–40.

56. Giacobello, F. *Larari Pompeiani. Iconografia e Culto dei Lari in Ambito Domestico*; Edizioni Universitarie di Lettere Economia Diritto: Milan, Italy, 2008.

57. Rossignani, M.P. L'ara e il suo contesto. In *L'ara Dipinta di Thaenae. Indagini sul Culto Martiriale nell'Africa Paleocristiana*; Cacitti, R., Legrottaglie, G., Pelizzari, G., Rossignani, M.P., Eds.; Viella: Rome, Italy, 2011.